Surface Topography: Metrology and Properties

PAPER

Axial alignment for high-precision interferometric measurements of steeply-curved spheres

RECEIVED
22 July 2015

REVISED
25 August 2015

ACCEPTED FOR PUBLICATION
4 September 2015

PUBLISHED
6 October 2015

Peter de Groot, Thomas Dresel and Bruce Truax

Zygo Corporation, Middlefield, CT 06455 USA

E-mail: peterd@zygo.com

Keywords: interferometry, Fizeau, alignment, optical metrology

Abstract

Incorrect positioning of a steeply-curved sphere along the optical axis of a laser Fizeau interferometer introduces a measurement error that is proportional to the cosine of the inclination angle of the ray trace within the cavity, and directly proportional to the misalignment. The standard metrology solution is to subtract a fitted parabola from the 3D image, which corrects for most of the error, but neglects higher terms. As a consequence, measurements of steeply curved parts may have residual errors resembling spherical aberration. Here we calculate the magnitude of the error and present it in a graphical format that allows for straightforward quantification of the residual error as a function of the measured quadratic or power term in the measured 3D surface form. While our recommendation is to employ automated alignment for best results, we also consider options for higher-order software corrections for geometric misalignments.

1. Introduction

A common test for spherical optics involves a Fizeau interferometer with a transmission sphere (TS) having a sufficiently high numerical aperture (NA) to capture the clear aperture of the test object, as shown in figure 1. Although established for many years as a high-precision metrology technique, there are a number of challenges when testing highly curved surfaces (e.g. f/0.65). One well-known problem is the effect of the spherical geometry on algorithms for mechanical phase shifting interferometry (PSI) [1]. However, even for systems and software for which phase-shift errors are not a significant issue, there remain uncertainties related to the geometric alignment of the interferometer cavity. Misalignments include tilt (or equivalently, lateral displacement) and longitudinal displacement along the optical axis (referred to as defocus or axial misalignment) away from the ideal confocal geometry. Of these misalignments, the most problematic is the defocus error, meaning an axial misalignment of the cavity.

When the test sphere in figure 1 is displaced longitudinally along the optical axis from the confocal position, circular fringes appear, usually approximated by a parabolic term in the reported surface figure. The parabolic surface—the 'power' term—is then removed to correct for the effect. At low NA (e.g. NA $<$ 0.25 or an f-number $>$2), this quadratic correction is sufficient. However, at higher NA and large amounts of defocus, additional geometrical effects may appear as residual errors, as shown in figure 2.

In a 1992 paper, Selberg noted that the net effect of defocus is given by the cosine of the inclination angle of the rays within the cavity with respect to the optical axis [2], which is only approximately corrected with a second-order fit. Lowman and Greivenkamp later documented defocus errors experimentally, although the dominant error source was ascribed to imperfections in the optical system [3]. In a more recent paper, Wesner *et al* described the exact form of the defocusing term as a function of NA, measured it experimentally, and recommended subtracting a corrective wave front based on this calculation [4]. Dongsheng Wang *et al* calculated the geometric effects of defocus and validated many of these experimentally [5]. Daodang Wang *et al* performed similar calculations, and proposed a solution based on successive wavefront measurements with a known relative defocus between them to solve simultaneously for the NA and the nominal focus offset [6]. Yang *et al* have proposed an alternative solution based on the averaging of four phase shifting algorithms with known relative offsets [7].

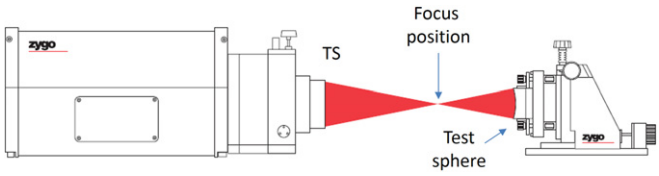

Figure 1. Laser interferometer with a Fizeau cavity formed by a test sphere and a transmission sphere (TS).

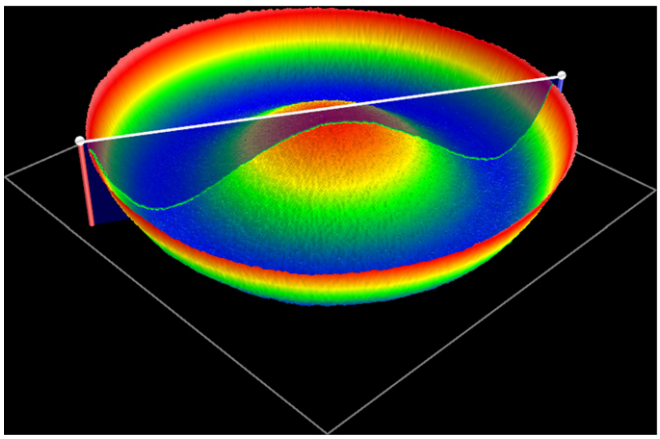

Figure 2. Experimental demonstration of measurement error in a Fizeau interferometer measurement of an f/0.65 spherical cavity (NA = 0.769). The cavity has been intentionally defocused (misaligned axially) by 3.0 μm. This image follows from removal of the best-fit parabola (peak–valley or PV = 1.0 μm), after subtraction of the nominal surface form as measured at the correct focus position. The PV is 0.056 μm, which is almost entirely due to uncorrected 4th-order geometric measurement errors in the misaligned cavity. The part diameter is 60 mm.

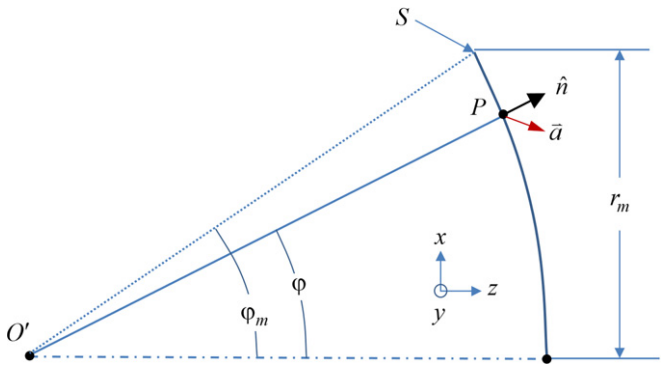

Figure 3. Geometry of a spherical interferometer cavity.

In spite of this prior work, the effect of focus misalignment is often neglected under the mistaken assumption that a parabolic fit is an exact solution, rather than an approximation that may be inadequate at high NA. In commercial software, standard practice is to use the parabolic approximation without the option of a higher-order fit. This is in part because a more exact fit requires information from the user—specifically, the NA of the confocal cavity—and routine measurements under less demanding circumstances do not require this level of attention. Even if an expert operator is aware of the limitations of the approximation, it is not always clear how well the system must be focused in order to stay within allowable uncertainty limits.

This paper reviews the calculation of surface form measurement errors related to defocus, and summarizes their magnitude. A principle result is a graphical representation of the allowable defocus, as measured using the parabolic fit, to achieve a desired level of measurement accuracy given the presence of higher-order error terms. We then outline a more accurate fitting algorithm for those applications that require further suppression of the residual error after

Table 1. Summary of the form error (one-half the wavefront error) introduced by cavity misalignment, for the case of small defocus in comparison with the test radius.

Coefficient	Functional term	Common description
C	1	Piston
a_x	$\rho_x A_N$	Tip
a_y	$\rho_y A_N$	Tilt
a_z	$\sqrt{1-\left(\rho_x A_N\right)^2-\left(\rho_y A_N\right)^2}$	Defocus

proper focus has been achieved within the mechanical limits of the system.

2. Calculation of the defocus error

Here we present a derivation using a straightforward vector analysis that differs from published derivations, while confirming these prior results. Referring to figure 3, let us assume that a ray enters point P on the sphere S and it comes in along the surface normal unit vector $\hat{n}$ given by

$$\hat{n} = n_x\hat{x} + n_y\hat{y} + n_z\hat{z} \tag{1}$$

where n_x, n_y, n_z are the vector components along the unit vectors $\hat{x}$, $\hat{y}$, $\hat{z}$ corresponding to the coordinates x, y, z, respectively. A misalignment will shift the point P (and with it the entire surface S) by the vector $\vec{a}$:

$$\vec{a} = a_x\hat{x} + a_y\hat{y} + a_z\hat{z}. \tag{2}$$

To first-order approximation, the optical path difference change because of this translation is twice the dot product of the normal unit vector $\hat{n}$ with the axial misalignment $\vec{a}$:

$$\mathrm{OPD} = 2a_x n_x + 2a_y n_y + 2a_z n_z. \tag{3}$$

Using φ as the elevation angle about the y-axis and defining θ as an angle about z for rotations within the x, y plane, we have

$$\begin{aligned} n_x &= \sin(\varphi)\cos(\theta) \\ n_y &= \sin(\varphi)\sin(\theta) \\ n_z &= \cos(\varphi), \end{aligned} \tag{4}$$

which we can rewrite as

$$\begin{aligned} n_x &= \rho_x A_N \\ n_y &= \rho_y A_N \\ n_z &= \sqrt{1-{\rho_x}^2{A_N}^2-{\rho_y}^2{A_N}^2}, \end{aligned} \tag{5}$$

where A_N is the NA and ρ_x, ρ_y are coordinates normalized to the part size r_m. Adding a constant term C and multiplying the result by $1/2$ shows that the effect on the local measured surface height is

$$\begin{aligned} h(\rho_x, \rho_y) = C + a_x\rho_x A_N + a_y\rho_y A_N \\ + a_z\sqrt{1-\left(\rho_x A_N\right)^2-\left(\rho_y A_N\right)^2}. \end{aligned} \tag{6}$$

The effect of the misalignment is to introduce an error described by four constant coefficients C, a_x, a_y, a_z corresponding to four ρ_x, ρ_y-dependent terms, as summarized in table 1.

3. Form and magnitude of the defocus error

Concentrating now on the defocus functional term in table 1, an expansion shows the 2nd-order term in radius ρ with the usually neglected higher-order terms:

$$\begin{aligned} \sqrt{1-\rho^2{A_N}^2} = 1 - \frac{1}{2}\rho^2{A_N}^2 - \frac{1}{8}\rho^4{A_N}^4 \\ - \frac{1}{16}\rho^6{A_N}^6 - \frac{5}{128}\rho^8{A_N}^8 + \ldots, \end{aligned} \tag{7}$$

where the radial location of the measurement point is

$$\rho = \sqrt{\rho_x^2 + \rho_y^2}. \tag{8}$$

The successive radius-dependent terms in equation (7) are all monotonically decreasing contributions in radius ρ. To minimize the peak–valley (PV) error using a parabolic fit, the residual error should be the same at the center $\rho = 0$ and at the edge $\rho = 1$. Defining a quadratic coefficient q and setting the residual at the edge equal to the residual at the center, we have

$$\sqrt{1-{A_N}^2} - q{A_N}^2 = 1. \tag{9}$$

Solving for q, introducing the scaling coefficient $-a_z$ and adding a constant piston offset so that the result is zero at the center $\rho = 0$, we arrive at a formula for the residual form error:

$$\begin{aligned} \varepsilon(\rho) = a_z\left[\left(\sqrt{1-{A_N}^2\rho^2}-1\right)\right. \\ \left. -\left(\sqrt{1-{A_N}^2}-1\right)\rho^2\right]. \end{aligned} \tag{10}$$

Figure 4 shows an example plot of the residual after minimum-PV parabolic fit to the form error in an f/0.65 spherical cavity with 3 microns of defocus. The minimization of the PV has the effect of pushing all of the residual errors to one side of zero.

The residual form error depends strongly on the NA of the spherical cavity. To determine the PV error dependence on NA, a first step is to identify the radial position $\rho_{\max}$ for which the residual error $\varepsilon(\rho_{\max})$ is greatest. To this end, we find the extrema of equation (10) by identifying the radius values for which the following derivative is zero:

$$\begin{aligned} \frac{\mathrm{d}\varepsilon}{\mathrm{d}\rho} = a_z\left[-\frac{{A_N}^2\rho}{\sqrt{1-{A_N}^2\rho^2}}\right. \\ \left. -2\left(\sqrt{1-{A_N}^2}-1\right)\rho\right]. \end{aligned} \tag{11}$$

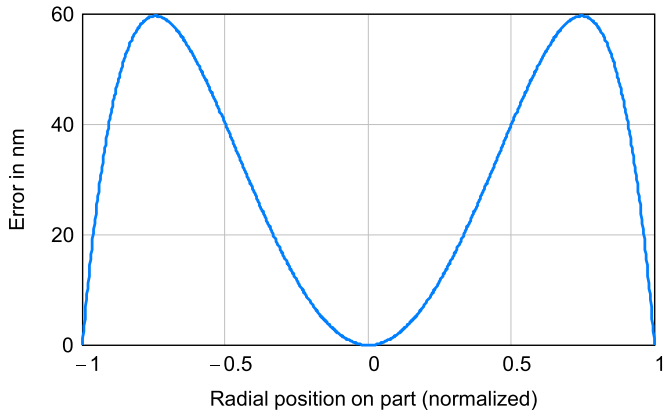

Figure 4. Cross section of the residual error in the surface profile of a defocused f/0.65 spherical cavity, after subtraction of a quadratic, parabolic fit and adjustment to minimize the PV error.

After some labor, this works out to

$$\rho^2_{\max}\left(A_N\right) = \left[\frac{1}{{A_N}^2} - \frac{{A_N}^2}{4\left(\sqrt{1-{A_N}^2}-1\right)^2}\right]. \tag{12}$$

This result inserted into equation (10) provides a closed form equation for the PV residual error ε_{res} as a function of NA, after subtraction of the best-fit parabola:

$$\varepsilon_{\text{res}} = a_z\left[\left(\sqrt{1-\left[1-\frac{{A_N}^4}{4\left(\sqrt{1-{A_N}^2}-1\right)^2}\right]}-1\right) - \left[\frac{\left(\sqrt{1-{A_N}^2}-1\right)}{{A_N}^2} - \frac{{A_N}^2}{4\left(\sqrt{1-{A_N}^2}-1\right)}\right]\right]. \tag{13}$$

The residual error after adjusting for minimum PV is proportional to the defocus amount a_z. Further, the overall shape of the residual error (see figure 4) is unaffected by the amount of defocus; rather, it is fundamentally related to the NA. We can therefore expect the RMS to increase quadratically with a_z, following the usual relationship between PV and RMS for a 4th-order surface. Assuming that we know the NA and the amount of defocus, equation (13) quantifies the expected residual error after subtraction of a quadratic (parabolic) fit and minimization of the PV in the software being used.

4. Minimizing the residual error

In practice, the usual method for correcting cavity misalignments is to evaluate the focus by visually observing circular fringes, followed by iteratively adjusting the test object position along the optical axis to minimize the measured focus term reported by the instrument software. The degree to which this can be accomplished is limited by the sensitivity of the parabolic term to defocus, the mechanical controls, and the patience of the system operator or the capabilities of an automated alignment. The general guidance is to do the best you can to minimize the defocus, with greater care when working with higher NA (smaller f-number).

Equation (13) calculates the PV if we know the exact amount of defocus a_z. Without precision displacement gauging, this can seem difficult to determine. However, it is straightforward to calculate the relationship between the defocus and the observed PV of the parabolic fitting term reported in the software. The expansion equation (7) shows that the quadratic term in radius ρ contributes a PV of

$$\varepsilon_q = {A_N}^2 a_z/2. \tag{14}$$

Therefore a convenient way to evaluate the focus adjustment requirement is to plot the ratio of the residual error of equation (13) to the measured PV of the directly measurable parabolic contribution of equation (14). The defocus distance cancels out because it is a linear coefficient for both calculations.

Figure 5 shows a graph of the ratio $\varepsilon_{\text{res}}/\varepsilon_q$ as a function of the f-number, which for a cavity geometry is equal to one-half the inverse of the NA. Knowing the nominal f-number of the TS and assuming that the measurement beam underfills the aperture of the part, figure 5 informs us of the residual PV error ε_{PV} caused by the parabolic approximation as a function NA and the degree of defocus as quantified by the PV of the fitted parabola. For example, suppose that we wish to keep the residual error resulting from the parabolic fit

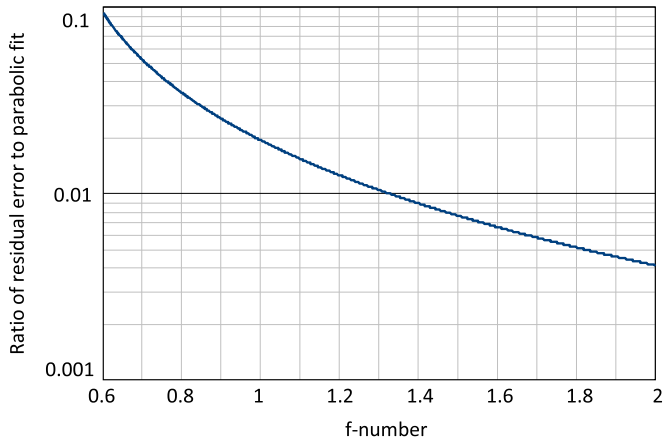

Figure 5. Ratio of the PV residual error caused by defocus after an approximate parabolic (quadratic or power) compensation to the measured PV of the parabolic term. This graph facilitates the estimation of the magnitude of the residual error for a range of f-numbers and the measured PV of the power term in standard instrument software.

to 10 nm, and the f-number is 1.3. Then from the graph, we can see that the observed PV of the parabolic fit (often referred to as the 'power' term) should be less than 1 μm, since the ratio is 0.01 or 1%. The focus adjustment requirement for the same 10 nm residual tightens to 0.14 μm when the f-number falls to 0.65.

5. Advanced fitting algorithms

For most practical applications, it is sufficient to use figure 5 as a guide and adjust the system until the required alignment tolerance is achieved. However, careful manual adjustment of the interferometer cavity to the sub-micron level requires skill, as well as mounting fixtures that have sufficient fine adjustment and mechanical stability. Automated systems with motorized alignment stages readily achieve PV focus terms below 50 nm in an f/0.65 cavity, reducing the residual error to below 5° nm [8]. Nonetheless, for some applications, even this level of adjustment may prove to be insufficient. If for example we are working with a 0.65 NA cavity and the allowable contribution from the defocus is just 1 nm, then the resulting requirement for 0.014 μm uncertainty in the axial alignment may not be achievable even with automated alignment. Even if the adjustment is feasible, it may not be stable over time. Here we document a higher-order fitting algorithm for correcting the alignment error, if this is needed to achieve a demanding uncertainty target.

As with all fitting routines, the idea is to determine the constant coefficients by a least-squares fit to the data map. The terms are piston, tip, tilt and defocus, with linear coefficients, as summarized in table 1. To make this clearer, we can rewrite the geometric error contribution of equation (6) using a vector v of coefficients:

$$h(\rho_x, \rho_y) = v_0 + v_1\rho_x + v_2\rho_y + v_3 f\left(\rho_x, \rho_y, NA\right), \tag{15}$$

where the linear coefficients are

$$\begin{aligned} v_0 &= C \\ v_1 &= a_x \\ v_2 &= a_y \\ v_3 &= a_z \end{aligned} \tag{16}$$

and

$$f\left(\rho_x, \rho_y, A_N\right) = \sqrt{1 - \left(\rho_x A_N\right)^2 - \left(\rho_y A_N\right)^2}. \tag{17}$$

The solution on a rectangular grid follows from the usual matrix methods for linear least-squares analysis:

$$\begin{pmatrix} v_0 \\ v_1 \\ v_2 \\ v_3 \end{pmatrix} = \begin{pmatrix} \langle 1 \rangle & \langle \rho_x \rangle & \langle \rho_y \rangle & \langle f \rangle \\ \langle \rho_x \rangle & \langle \rho_x^2 \rangle & \langle \rho_x \rho_y \rangle & \langle \rho_x \rho_y f \rangle \\ \langle \rho_y \rangle & \langle \rho_x \rho_y \rangle & \langle \rho_y{}^2 \rangle & \langle \rho_y f \rangle \\ \langle f \rangle & \langle \rho_x f \rangle & \langle \rho_y f \rangle & \langle f^2 \rangle \end{pmatrix}^{-1} \times \begin{pmatrix} \langle H \rangle \\ \langle \rho_x H \rangle \\ \langle \rho_y H \rangle \\ \langle f H \rangle \end{pmatrix} \tag{18}$$

where

$$\begin{aligned} \langle \rho_x f \rangle &= \sum_{x,y} \rho_x f\left(\rho_x, \rho_y, A_N\right) \\ \langle f \rangle &= \sum_{x,y} f\left(\rho_x, \rho_y, A_N\right) \end{aligned} \tag{19}$$

and the sums are over all valid pixels in the measured 3D height image $H\left(\rho_x, \rho_y\right)$. This more exact fitting algorithm is equivalent to a spherical fit in deviation

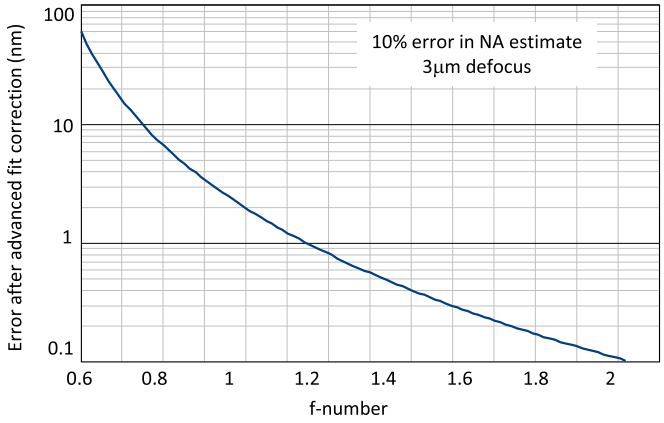

Figure 6. The measurement error resulting from an overestimation of the NA in the presence of 3 microns of defocus, after correction using the advanced fitting algorithm.

space, constrained to a fixed diameter in the included angle.

In principle, this more advanced fitting algorithm fully compensates for the axial alignment error described in sections 2 and 3. However, an important observation is that we need to know the value of A_N in order to calculate the defocus function f. A solution is to determine the NA from the known geometry of the system. This requires some care if the test part underfills the aperture, since in this case simply using the f-number of the transmission sphere would lead to an overestimate of the NA. An alternative is to determine the NA independently from other factors by making multiple measurements at different defocus positions with a known offset between them. Alternatives to the proposed least-squares approach are certainly possible, including splines or other fitting techniques, although in all cases it is necessary to know or to empirically solve for the NA to interpret the results.

Figure 6 shows the sensitivity of the advanced fitting algorithm to errors in the estimated NA. This graph is for the case of a 3 μm axial misalignment, which is quite large. Given that the error scales linearly with defocus, reasonable care in aligning the cavity can significantly relax the accuracy requirements for estimating the NA for the advanced fitting method. A conclusion therefore is that even when we are using this more exact error removal, it is to our advantage to minimize the axial misalignment.

The advanced fitting algorithm and the measurement of high-NA optics generally are subject to other potentially significant sources of error beyond axial misalignment. Evans and Bryan provided an analysis and methodology for compensating errors introduced by nonzero fringe densities in phase-measuring interferometers [9]. Retrace errors and field distortion are of particular concern with highly-sloped surfaces as the lateral calibration or overall field magnification. At high levels of precision, the data acquisition and analysis technique comes under scrutiny, including cross-coupling of errors related to mechanical phase shifting interferometry and multiple reflections in the Fizeau cavity [10]. It is equally important to consider the instrument transfer function, including the effects of imaging errors and phase distortions at high spatial frequencies [11, 12]. Although it is beyond the scope of this paper, a full accounting of these errors is essential for a complete uncertainty analysis of high-precision interferometric measurements of steeply curved spheres.

6. Conclusion

Precision measurements of steeply curved spherical surfaces with laser interferometry require care in aligning the interferometer components to limit the contribution of apparent form deviations related to focus. Once a sufficient level of alignment has been achieved, a parabolic fit and remove suppress most of the focus effect, with some residual errors related to higher-order terms that are neglected in the parabolic approximation.

In the present work, we quantify the residual errors and relate them to the PV departure of the parabolic fit—often referred to as the power term as reported in standard instrument software for this application. The results of figure 5 provide a guideline for determining the degree of care in aligning the interferometer to reach specified uncertainty goals. For demanding applications, we recommend motorized staging to automatically align the interferometer cavity.

Finally, we outline a least-squares spherical fit that is effective if the NA of the system is well known or can be characterized *in situ*. This algorithm may be useful to relax alignment requirements and to reach highest precision; however, it remains important to minimize the axial misalignment, to relax requirements on the estimate of the NA.

Acknowledgments

The authors would like to thank Barbara Carr for setting up the experiment leading to figure 2, and Shiguang Wang for modeling the interferometer in optical design software.

References

[1] Moore R C and Slaymaker F C 1980 Direct measurement of phase in a spherical-wave Fizeau interferometer *Appl. Opt.* **19** 2196–200
[2] Selberg L A 1992 Radius measurement by interferometry *Opt. Eng.* **31** 1961–6
[3] Lowman A E and Greivenkamp J E 1996 Interferometer errors due to the presence of fringes *Appl. Opt.* **35** 6826–8
[4] Wesner J, Heil J and Heuck H M 2009 High NA absolute Fizeau phase shifting interferometry *DGaO Proc.* **110** C16
[5] Wang D, Wang K, Shen Y and Peng J 2010 Error analysis of spherical ultra-precision measurement *5th Int. Symp. on Advanced Optical Manufacturing and Testing Technologies: Optical Test and Measurement Technology and Equipment* ed Y Zhang, J M Sasian, L Xiang and S To Proc.(*SPIE*) **7656** 76560O–1
[6] Wang D, Yang Y, Chen C and Zhuo Y 2011 Misalignment aberrations calibration in testing of high-numerical-aperture spherical surfaces *Appl. Opt.* **50** 2024–31
[7] Yang Z, Gao Z, Wang S, Wang X and Shi Q 2015 Sub-nanometer misalignment aberrations calibration of the Fizeau interferometer for high-numerical-aperture spherical surface ultra-precision measurement *Optik* **126** 1865
[8] Automated cavity alignment is available on the ZYGO Verifire™ laser interferometer (www.zygo.com/?/met/interferometers/verifire/asphere/)
[9] Evans C J and Bryan J B 1993 Compensation for errors introduced by nonzero fringe densities in phase-measuring interferometers *CIRP Ann* **42** 577–80
[10] de Groot P J 2014 Correlated errors in phase-shifting laser Fizeau interferometry *Appl. Opt.* **53** 4334–42
[11] Doerband B and Hetzler J 2005 Characterizing lateral resolution of interferometers: The height transfer Function (HTF) ed A Duparré, B Singh and Z-H Gu *Advanced Characterization Techniques for Optics, Semiconductors, and Nanotechnologies II Proc.*(SPIE) vol 5878 p 587806
[12] Colonna de Lega X and de Groot P 2012 Lateral resolution and instrument transfer function as criteria for selecting surface metrology instruments *Optical Fabrication and Testing, OSA Proc. Optical Fabrication and Testing* OTu1D